Joint International Topical Meeting on Mathematics & Computation and Supercomputing in Nuclear Applications (M&C + SNA 2007)
Monterey, California, April 15-19, 2007, on CD-ROM, American Nuclear Society, LaGrange Park, IL (2007)

DRAGON EVALUATION OF THE BENCHMARK FOR THE DOPPLER REACTIVITY DEFECT

J. Le Mer and G. Marleau
Institut de génie nucléaire, École Polytechnique de Montréal
C.P. 6079, succ. Centre-ville, Montréal, Québec, CANADA H3C 3A7
joel.le-mer@polymtl.ca; guy.marleau@polymtl.ca

ABSTRACT

A set of computational benchmarks for the Doppler reactivity defect for fuel pin cells was submitted by R. D. Mosteller. It includes UO_2 fuel, reactor-recycle mixed-oxide(MOX) fuel and weapons-grade MOX fuel with several enrichments. This paper describes the choices of computations and the results of these benchmarks with DRAGON. We will show that for the calculation of Doppler defect, we do not need a mesh as fine as the one we use for the neutron flux calculation. Moreover we find out that different libraries can give significantly different results for the Doppler defect.

Key Words: Doppler Defect, Collision Probabilities method, Dragon

1. INTRODUCTION

Two computational benchmarks have been proposed in 1991 to assess the Doppler coefficient of reactivity for 2-D PWR fuel cells [1, 2]. The fact that they had a very simple geometry made it possible for a large number of organizations to use their cell codes and produce reliable results. However, they were limited to UO_2 and MOX fuels with relatively low enrichment.

A new series of computational benchmarks for Doppler reactivity defect has been proposed by R. Mosteller aiming at extending the previous studies [3]. These benchmarks simulate the Doppler defect between hot zero power (HZP) and hot full power (HFP) for 16 different types of fuels in a PWR lattice. For these calculations the temperature of the cladding and the moderator remains at 600 K for both conditions. The fuel temperature is assumed to rise from 600 K at HZP to 900 K at HFP leading to a 0.001 % increase in the radial dimension of the fuel. The moderator is borated water and contains 1400 PPM of boron. The clad is supposed to be pure natural zirconium.

The reference pin cell is that described in Fig. 1 where, from the center to the exterior, the regions are: the fuel (with external radius of 0.39398 cm and 0.39433 cm respectively for HZP and HFP), the gap (with external radius of 0.40226 cm), the clad (with external radius of 0.45972 cm) and finally the coolant. The total width of the cell is 1.26678 cm.

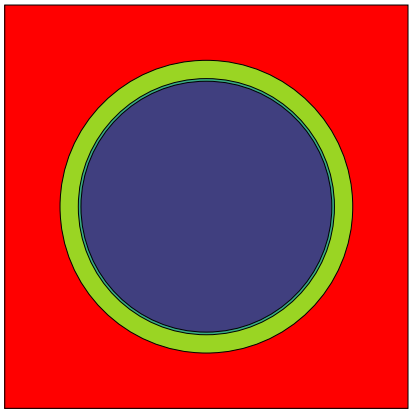

Figure 1. Pin Cell

The 16 types of fuel considered are: 7 conventional UO_2 fuels with enrichment ranging from natural uranium to 5.0 wgt%, 5 reactor-recycle MOX fuels with enrichment ranging from 1.0 to 8.0 wgt% and 4 weapons-grade MOX fuels with enrichment ranging from 1.0 to 6.0 wgt%.

These two dimensional benchmarks will be analyzed here with the lattice code DRAGON [4] developed at École Polytechnique de Montréal. A multigroup solution of the integral transport equation will be obtained using the method of collision probabilities (CP). Results obtained for a variety of microscopic cross section libraries, including ENDF/B-VI and JEFF-3.1 WLUP libraries [5] will be presented and discussed.

2. DRAGON CELL MODEL

DRAGON is a lattice cell code that can use both the method of collision probability and the method of characteristics to solve the neutron transport equation in infinite heterogeneous cells. Here we will consider only the method of collision probabilities to integrate a multigroup solution of the integral transport equation. Two types of boundary conditions are also available: white boundary conditions where the angular flux on the surface is assumed isotropic and mirror like boundary conditions. For the case where white boundary conditions are selected, the standard tracking procedure for collision probability calculations is used. For the case where mirror like boundary are considered, the tracking lines are selected in such a way that they are cyclic over the cell [6].

The resonance self-shielding calculations were performed using an equivalence approach, the improved Stamm'ler method [7], with the fuel-to fuel collision probabilities computed for the exact geometry. Since the geometry is fully symmetric a 1/8 description of the cell was modeled and we have used 3 subdivisions along the Cartesian side and we did not further subdivide the annular fuel region, which leads to a problem with 7 regions and 2 surfaces for the resonance self-shielding calculation as can be seen in Fig. 2. We performed two sets of calculation: with and without Livolant and Jeanpierre normalization where the resonance flux is computed using the escape function interpolated at the self-shielded cross section rather that the averaged microscopic dilution cross section. The default option in DRAGON is not to use Livolant and Jeanpierre normalization sheme. But previous calculations have shown that the Livolant and Jeanpierre normalization is usually more accurate for PWR type reactor.

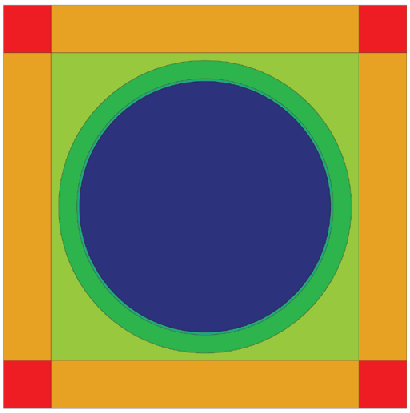

Figure 2. Pin Cell

DRAGON can solve the collision probability equations for the flux using the simple 4 region geometry problem of Fig. 1 but this solution is not accurate because the flat source approximation is not satisfied in this case. Therefore we had to define a fine geometry for the transport calculation.

We will define three different geometries that can be used by different tracking modules included in DRAGON for the flux calculation.

- For our basic model we use two different geometries for the HFP and the HZP fuels. This geometry is supposed to be less accurate than the next ones but it is much faster to analyse and the results are relatively acurate as we will see. This model includes 13 subdivisions along the Cartesian side and 2 radial subdivisions of the fuel region to ensure k_{eff} convergence. The resulting problem that is solved involves 48 regions and 7 surfaces per energy groups for 1/8 of the cell (see Fig. 3a). The line spacing of the tracking is 0.002 cm.
- Two more complicated models were also defined in such a way that there is only one geometry for the HFP and HZP fuels. This creates a very thin region that will be filled with fuel or air respectively for the HFP and HZP fuels but we have consistent models for calculations at HZP and HFP. In order to lower the number of regions, we will follow the geometry of the cell for the discretizations.
  - The first option consists of using cylindrical regions in the coolant and adding Cartesian discretization on the borders. Based on our studies the mesh discretization that would ensure spatial convergence of the neutron flux consists in a model with 6 subdivisions along the Cartesian sides on each side of the cell for the coolant region with 5 radial subdivisions inside the fuel region and 6 radial subdivisions outside the fuel region. The resulting problem that is solved involves 62 regions and 7 surfaces per energy groups for 1/8 of the cell (see Fig. 3b).
  - The other option is to use bloc-by-bloc discretization which is possible thanks to the new module of DRAGON version 3.05. Based on our studies the mesh discretization that ensures spatial convergence of the neutron flux consists in a model with 30 subdivisions along the Cartesian sides of the cell for the coolant region with an additional 5 radial subdivisions for the fuel region. The resulting problem involves 93 regions and 15 surfaces per energy groups for 1/8 of the cell (see Fig. 3c).

A very fine tracking was then required to ensure that the region volumes and surface areas could be evaluated numerically from the tracks with errors below 1%. Here the line spacing varied between 0.001 and 0.0005 cm.

For all these geometries, the angular quadrature consisted of 8 azimuthal angles (gaussian quadrature) and 4 polar directions (Gauss-Legendre quadrature) for the mirror like boundary and 32 angles azimuthal angles (trapezoïdal quadrature) for the white boundary.

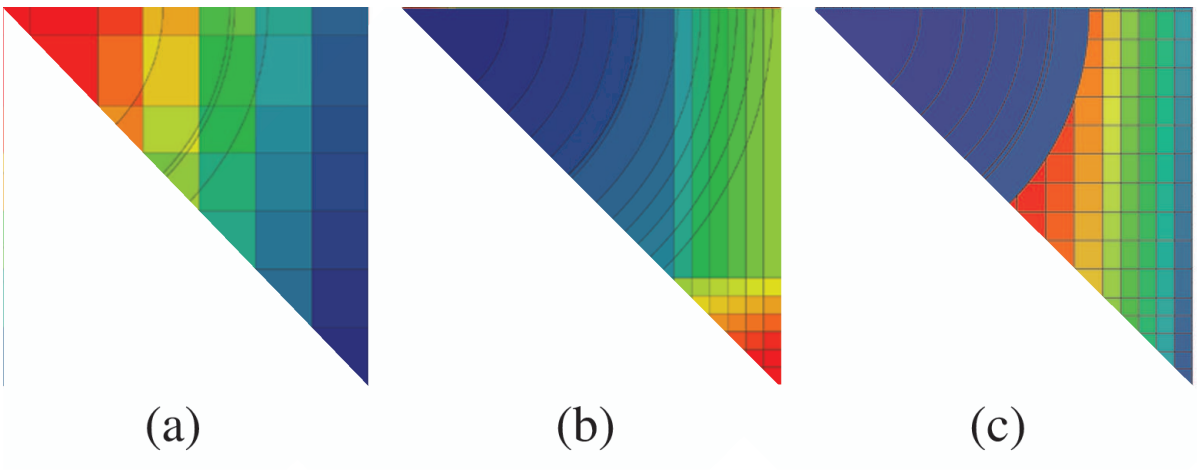

Figure 3. Pin Cell

3. CROSS SECTION LIBRARIES

The code DRAGON can read various microscopic cross section library formats including those compatible with WIMS-D4 [8] and WIMS-AECL [9]. Accordingly, we had access to a number of different libraries including those generated by the IAEA as a result of the "WIMS Library Update Program" (WLUP). The main WLUP libraries we considered are:

- iaea (69 groups) and iaeagx (172 groups) cross section libraries that include more than 170 isotopes from selected evaluated nuclear data files. These libraries were extensively validated over 200 benchmark cases.
- jeff31 (69 groups) and jeff31gx (172 groups), which are similar to the iaea and iaeagx libraries respectively, except that all the isotopes were extracted from JEFF-3.1.
- endfb6 (69 groups) and endfb6gx (172 groups), which are again similar to the iaea and iaeagx libraries, but all the isotopes are now extracted from revision 8 of ENDF/B-VI.

An 89 groups WIMS-AECL format library, called e6wlib, was also used for testing. We will not present the results in this paper because they are based on a very old release of ENDF/B-VI.

4. RESULTS

We choose to take as the reference the results obtained with the library endfgx. Mirror like boundaries, self-shielding with the Livolant-Jeanpierre normalization and the geometry described in Fig. 3c were selected. The Doppler defect in this case is given in Tables I to III (see appendix). The first observation is that there are no direct link between the Doppler defect and the k_{eff}: the Doppler defect usually decreases as the enrichment increases but it is not a general rule, which proves the necessity to improve our knowledge with this kind of benchmarks for higher enrichments.

The Doppler defects computed with the other libraries for the same conditions case are given in Tables IV to IX (see appendix). From these results, we can make some statements:

- The use of the same library data but with different number of energy groups indicates the 69 energy group library is adequate for conventional UO_2 fuel and weapons-grade mixed oxide fuel; the difference being under 1.4% for the Doppler coefficient. On the other hand, the 172 energy group results seem to be more accurate for the reactor-recycle mixed-oxide where differences of up to 8.5% on Doppler coefficient are observed. This observation is true with the three sets of libraries. These large differences would seem to indicate that the ^{241}Pu and ^{242}Pu cross sections in the 69 energy group libraries are inadequate for this benchmark.

- If we compare results from endfb6gx and jeff31gx, we found that there are some significant differences between the k_{eff}: the k_{eff} found with jeff31gx is higher than the one found with endfb6gx with a difference of up to 200 pcm. Nevertheless, the Doppler coefficient are very close with these two libraries: For UO_2 and weapons-grade MOX fuels, the Doppler defect with jeff31gx is up to 1% higher than the one obtained with endfb6gx. For reactor-recycled MOX fuels, the Dopller defect with jeff31gx is underevaluated by up to 1.3% as compared to the endfb6gx results.

- In general, the difference between endfb6gx and iaeagx is higher than between endfb6gx and jeff31gx. For UO_2 fuels, the k_{eff} found with iaeagx is higher than the one found with endfb6gx by up to 1100 pcm (the difference getting higher with enrichment). For MOX fuels, the endfb6gx k_{eff} are higher than the ones found with iaeagx by up to 600 pcm (the difference getting higher with MOX contents). The Doppler coefficient is always lower when calculated with iaeagx than when calculated with endfb6gx. These differences are around 1% for UO_2 and weapons-grade MOX fuels and between 2% and 4% for the reactor-recycle MOX. Those greater differences between endfb6gx and iaeagx than between endfb6gx and jeff31gx is because iaeagx takes its cross section in different evaluations. For instance, the cross section of ^{235}U comes from ENDF/B-VI release 8 but the cross sections of the isotopes of the plutonium come from FOND-2 release 2 which could lead to some problem of adjustment between cross section.

We repeated the same calculations with all the geometries and options we have presented in section 2. Here we are going to concentrate on the results obtained with endfgx. Every conclusions are also relevant for the other libraries.

- The results calculated with the geometries of Fig. 3a and 3b are within $\pm$ 0.3% for the Doppler coefficient calculated with the reference case which is within the precision of our calculations. We can see that the use of a very fine mesh is not useful for Doppler defect calculation.

- Mirror like boundaries conditions are much more expensive in CPU time but they provide more reliable results. A $\pm$ 1% error is observed when the white boundary conditions are considered. This difference is below that observed when different libraries are compared. For the case when CPU time is at a premium this option seems to be perfectly adequate.
- As we said previously, we have also performed the calculation without Livolant and Jeanpierre normalisation sheme (see column "no LJ" in Tables X to XII). In our benchmark, this choice creates an offset between -6 and -12 mK for the k_{eff} but only a difference between +3.5% and +5% of the Doppler Defect.
- If we consider that there is no dilatation of fuel between HZP and HFP (see column "no dilatation" in Tables X to XII), the Doppler coefficient is 4% higher for the natural uranium fuel but the difference is lowered when the enrichment grows. For high enrichment, the difference changes sign and becomes -2%.

5. CONCLUSIONS

The first important fact we can observe is the need of a fine discretization of the geometry and of the tracking to have converged results. Nevertheless, the error on the Doppler defect created by using two different geometries for HZP and HFP is small. Selecting a discretization that ensures neutron flux convergence is too excessive for the calculation of the Doppler defect and if CPU time is important we could have chosen to performed the calculations with the discretization of Fig. 3a.

The difference created by using different libraries leads to very important differences on k_{eff} (more than 1200 pcm) but the differences in the Doppler coefficients remain under 0.3 pcm.K^{-1} (under 0.6 pcm.K^{-1} if we consider the WIMS-AECL format library). Nevertheless, these differences are relevant and even with the three 172 energy group libraries, it can mean 4% difference for Doppler coefficient.

The use of a large number of librairies shows that reactor-recycle MOX fuels are more sensitive to library than the other fuels. While the use of 69 energy group libraries are sufficient for UO_2 and weapons-grade MOX (error under 1%), we recommand to use 172 energy group libraries to compute the reactor-recyle MOX fuel cases.

ACKNOWLEDGEMENTS

This work was supported by the Conseil de Recherches en Sciences Naturelles et en Génie du Canada and Électricité de France.

REFERENCES

[1] R. D. Mosteller, L. D. Eisenhart, R. C. Little, W. J. Eich and J. Chao, "Benchmark Calculations for the Doppler Coefficient of Reactivity," *Nucl. Sci. Eng.*, **107**, pp. 265-271 (1991).

[2] R. D. Mosteller, J. T. Holly, and L. A. Mott, "Benchmark Calculations for the Doppler Coefficient of Reactivity in Mixed-Oxide Fuel,"*Proceedings of the International Topical Meeting on Advances in Mathematics, Computations, and Reactor Physics*, CONF-910414, pp. 9.2 1-1.2 1-12, Pittsburgh, Pennsylvania (1991).

[3] R. D. Mosteller, "Computational Benchmarks for the Doppler Reactivity Defect," LA-UR-06-2968, Los Alamos National Laboratory (2006).

[4] G. Marleau, A. Hébert and R. Roy, *A User Guide for DRAGON 3.05*, Report IGE-174 Rev. 6, Institut de génie nucléaire, École Polytechnique de Montréal (2006).

[5] "WIMS Library Update Program," http://www-nds.iaea.org/wimsd/ (2005).

[6] R. Roy, G. Marleau and A. Hébert, "A Cyclic Tracking Procedure for Collision Probability Calculation in 2-D Lattices," *International Topical Meeting Advances in Mathematics, Computations and Reactor Physics*, Pittsburgh, PA, pp. 2.2.4.1-2.2.4.14 (1991).

[7] A. Hébert and G. Marleau, "Generalization of the Stamm'ler Method for the Self-Shielding of Resonant Isotopes in Arbitrary Geometries", *Nucl. Sci. Eng.*, **108**, 230 (1991).

[8] J. R. Askew, F. J. Fayers and P. B. Kemshell, "A General Description of the Lattice Code WIMS," *J. Brit. Nucl. Energy Soc.*, **5**, pp. 564 (1966).

[9] J. V. Donnelly, "WIMS-CRNL, A User's Manual for the Chalk River Version of WIMS,", Atomic Energy of Canada Limited, AECL-8955, (1986).

APPENDIX

The results presented in Tables I to IX where obtained with the geometry of the Fig. 3c assuming that the Livolant-Jeanpierre normalization is applied in our self shielding calculations:

- calculations performed using the endfb6gx WLUP library (172 groups) and the endfb6 WLUP library (69 groups) and Livolant and Jeanpierre normalization are presented in Table I to III respectively for the UO2, reactor-recycle MOX and weapons-grade MOX.
- calculations performed using the jeff31gx WLUP library (172 groups) and the jeff31 WLUP library (69 groups) and Livolant and Jeanpierre normalization are presented in Table IV to VI
- calculations performed using the iaeagx WLUP library (172 groups) and the iaea WLUP library (69 groups) and Livolant and Jeanpierre normalization are presented in Table VII to IX respectively for the UO2, reactor-recycle MOX and weapons-grade MOX.

The results presented in the column "no LJ" of the Tables X to XII where obtained assuming with the same conditions as in the reference calculation but the Livolant-Jeanpierre normalization is not applied in our self shielding calculations. The relative error in the Doppler coefficient is given between this case and the reference case.

The results presented in the column "no dilatation" of the Tables X to XII where obtained assuming the same conditions as in the reference case but that there is no dilatation of the fuel between HZP and HFP. The relative error in the Doppler coefficient is given between this case and the reference case.

Results for endfb6gx and endfb6:

Table I. UO_2 fuels

	endfb6gx				endfb6			
Enrichment (wgt.%)	HZP k_{eff}	HFP k_{eff}	$\Delta\rho$ (pcm)	$\Delta\rho/\Delta T$ (pcm/K)	HZP k_{eff}	HFP k_{eff}	$\Delta\rho$ (pcm)	$\Delta\rho/\Delta T$ (pcm/K)
0.711	0.66364	0.65711	-1498	-4.99	0.66263	0.65612	-1499	-5.00
1.6	0.95712	0.94790	-1016	-3.39	0.95558	0.94637	-1019	-3.40
2.4	1.09479	1.08450	-866	-2.89	1.09275	1.08244	-872	-2.91
3.1	1.17255	1.16173	-794	-2.65	1.17011	1.15924	-801	-2.67
3.9	1.23510	1.22390	-741	-2.47	1.23221	1.22094	-749	-2.50
4.5	1.27054	1.25914	-712	-2.37	1.26732	1.25584	-721	-2.40
5.0	1.29487	1.28337	-692	-2.31	1.29142	1.27983	-701	-2.34

Table II. Reactor-recycle MOX fuels

	endfb6gx				endfb6			
MOX Content (wgt.%)	HZP k_{eff}	HFP k_{eff}	$\Delta\rho$ (pcm)	$\Delta\rho/\Delta T$ (pcm/K)	HZP k_{eff}	HFP k_{eff}	$\Delta\rho$ (pcm)	$\Delta\rho/\Delta T$ (pcm/K)
1.0	0.94209	0.93106	-1257	-4.19	0.94739	0.93682	-1191	-3.97
2.0	1.01742	1.00493	-1221	-4.07	1.02665	1.01489	-1129	-3.76
4.0	1.07193	1.05880	-1157	-3.86	1.08412	1.07181	-1059	-3.53
6.0	1.10026	1.08710	-1100	-3.67	1.11256	1.10017	-1012	-3.37
8.0	1.12349	1.11043	-1047	-3.49	1.13489	1.12248	-974	-3.25

Table III. Weapons-grade MOX fuels

	endfb6gx				endfb6			
MOX Content (wgt.%)	HZP k_{eff}	HFP k_{eff}	$\Delta\rho$ (pcm)	$\Delta\rho/\Delta T$ (pcm/K)	HZP k_{eff}	HFP k_{eff}	$\Delta\rho$ (pcm)	$\Delta\rho/\Delta T$ (pcm/K)
1.0	1.08535	1.07493	-893	-2.98	1.08435	1.07396	-891	-2.97
2.0	1.17496	1.16252	-911	-3.04	1.17426	1.16189	-907	-3.02
4.0	1.24289	1.22916	-899	-3.00	1.24240	1.22882	-890	-2.97
6.0	1.27949	1.26548	-866	-2.89	1.27904	1.26513	-859	-2.86

Results for jeff31gx and jeff31:

Table IV. UO_2 fuels

	jeff31gx				jeff31			
Enrichment (wgt.%)	HZP k_{eff}	HFP k_{eff}	$\Delta\rho$ (pcm)	$\Delta\rho/\Delta T$ (pcm/K)	HZP k_{eff}	HFP k_{eff}	$\Delta\rho$ (pcm)	$\Delta\rho/\Delta T$ (pcm/K)
0.711	0.66392	0.65733	-1510	-5.03	0.66277	0.65619	-1511	-5.04
1.6	0.95814	0.94885	-1022	-3.41	0.95647	0.94718	-1025	-3.42
2.4	1.09588	1.08552	-871	-2.90	1.09373	1.08334	-877	-2.92
3.1	1.17362	1.16272	-799	-2.66	1.17106	1.16011	-806	-2.69
3.9	1.23609	1.22480	-745	-2.48	1.23309	1.22173	-754	-2.51
4.5	1.27146	1.25999	-716	-2.39	1.26813	1.25656	-726	-2.42
5.0	1.29573	1.28415	-696	-2.32	1.29217	1.28047	-707	-2.36

Table V. Reactor-recycle MOX fuels

	jeff31gx				jeff31			
MOX Content (wgt.%)	HZP k_{eff}	HFP k_{eff}	$\Delta\rho$ (pcm)	$\Delta\rho/\Delta T$ (pcm/K)	HZP k_{eff}	HFP k_{eff}	$\Delta\rho$ (pcm)	$\Delta\rho/\Delta T$ (pcm/K)
1.0	0.94297	0.93195	-1253	-4.18	0.94754	0.93686	-1203	-4.01
2.0	1.01910	1.00670	-1209	-4.03	1.02740	1.01550	-1141	-3.80
4.0	1.07421	1.06117	-1144	-3.81	1.08551	1.07305	-1069	-3.56
6.0	1.10248	1.08939	-1090	-3.63	1.11407	1.10153	-1022	-3.41
8.0	1.12541	1.11240	-1040	-3.47	1.13626	1.12370	-984	-3.28

Table VI. Weapons-grade MOX fuels

	jeff31gx				jeff31			
MOX Content (wgt.%)	HZP k_{eff}	HFP k_{eff}	$\Delta\rho$ (pcm)	$\Delta\rho/\Delta T$ (pcm/K)	HZP k_{eff}	HFP k_{eff}	$\Delta\rho$ (pcm)	$\Delta\rho/\Delta T$ (pcm/K)
1.0	1.08588	1.07537	-900	-3.00	1.08476	1.07428	-900	-3.00
2.0	1.17612	1.16355	-918	-3.06	1.17527	1.16277	-915	-3.05
4.0	1.24448	1.23060	-906	-3.02	1.24380	1.23010	-895	-2.98
6.0	1.28104	1.26689	-872	-2.91	1.28040	1.26631	-869	-2.90

Results for iaeagx and iaea:

Table VII. UO_2 fuels

	iaeagx				iaea			
Enrichment (wgt.%)	HZP k_{eff}	HFP k_{eff}	$\Delta\rho$ (pcm)	$\Delta\rho/\Delta T$ (pcm/K)	HZP k_{eff}	HFP k_{eff}	$\Delta\rho$ (pcm)	$\Delta\rho/\Delta T$ (pcm/K)
0.711	0.66826	0.66170	-1484	-4.95	0.66709	0.66056	-1484	-4.95
1.6	0.96399	0.95471	-1008	-3.36	0.96230	0.95303	-1011	-3.37
2.4	1.10293	1.09258	-860	-2.87	1.10075	1.09037	-865	-2.88
3.1	1.18164	1.17073	-789	-2.63	1.17905	1.16809	-795	-2.65
3.9	1.24515	1.23385	-736	-2.45	1.24211	1.23073	-744	-2.48
4.5	1.28125	1.26975	-707	-2.36	1.27787	1.26628	-717	-2.39
5.0	1.30612	1.29450	-687	-2.29	1.30249	1.29076	-698	-2.33

Table VIII. Reactor-recycle MOX fuels

	iaeagx				iaea			
MOX Content (wgt.%)	HZP k_{eff}	HFP k_{eff}	$\Delta\rho$ (pcm)	$\Delta\rho/\Delta T$ (pcm/K)	HZP k_{eff}	HFP k_{eff}	$\Delta\rho$ (pcm)	$\Delta\rho/\Delta T$ (pcm/K)
1.0	0.94105	0.93031	-1227	-4.09	0.94602	0.93557	-1181	-3.94
2.0	1.01468	1.00257	-1191	-3.97	1.02347	1.01186	-1122	-3.74
4.0	1.06791	1.05521	-1127	-3.76	1.07964	1.06754	-1050	-3.50
6.0	1.09575	1.08310	-1066	-3.55	1.10766	1.09558	-995	-3.32
8.0	1.11878	1.10623	-1014	-3.38	1.12984	1.11781	-953	-3.18

Table IX. Weapons-grade MOX fuels

	iaeagx				iaea			
MOX Content (wgt.%)	HZP k_{eff}	HFP k_{eff}	$\Delta\rho$ (pcm)	$\Delta\rho/\Delta T$ (pcm/K)	HZP k_{eff}	HFP k_{eff}	$\Delta\rho$ (pcm)	$\Delta\rho/\Delta T$ (pcm/K)
1.0	1.08318	1.07284	-890	-2.97	1.08204	1.07173	-889	-2.96
2.0	1.17056	1.15829	-905	-3.02	1.16970	1.15750	-901	-3.00
4.0	1.23660	1.22312	-891	-2.97	1.23593	1.22257	-885	-2.95
6.0	1.27254	1.25879	-858	-2.86	1.27190	1.25823	-854	-2.85

Results for endfb6gx, without Livolant-Jeanpierre normalization in the left columns and without dilatation of the fuel in the right columns.

Table X. UO_2 fuels

	no LJ				no dilatation			
Enrichment (wgt.%)	HZP k_{eff}	HFP k_{eff}	$\Delta\rho/\Delta T$ (pcm/K)	Relative error	HZP k_{eff}	HFP k_{eff}	$\Delta\rho/\Delta T$ (pcm/K)	Relative error
0.711	0.65726	0.65057	-5.22	4.6%	0.66364	0.65683	-5.21	4.3%
1.6	0.94791	0.93844	-3.55	4.8%	0.95712	0.94772	-3.45	2.0%
2.4	1.08449	1.07392	-3.03	4.8%	1.09479	1.08440	-2.92	1.0%
3.1	1.16177	1.15065	-2.77	4.8%	1.17255	1.16169	-2.66	0.4%
3.9	1.22402	1.21251	-2.59	4.7%	1.23510	1.22391	-2.47	-0.1%
4.5	1.25934	1.24763	-2.48	4.6%	1.27054	1.25919	-2.36	-0.4%
5.0	1.28361	1.27179	-2.41	4.6%	1.29487	1.28343	-2.30	-0.5%

Table XI. Reactor-recycle MOX fuels

	no LJ				no dilatation			
MOX Content (wgt.%)	HZP k_{eff}	HFP k_{eff}	$\Delta\rho/\Delta T$ (pcm/K)	Relative error	HZP k_{eff}	HFP k_{eff}	$\Delta\rho/\Delta T$ (pcm/K)	Relative error
1.0	0.93295	0.92169	-4.36	4.2%	0.94209	0.93107	-4.19	-0.1%
2.0	1.00788	0.99517	-4.23	3.8%	1.01742	1.00506	-4.03	-1.0%
4.0	1.06268	1.04931	-4.00	3.7%	1.07193	1.05899	-3.80	-1.5%
6.0	1.09155	1.07815	-3.79	3.4%	1.10026	1.08727	-3.62	-1.4%
8.0	1.11536	1.10205	-3.61	3.4%	1.12349	1.11057	-3.45	-1.1%

Table XII. Weapons-grade MOX fuels

	no LJ				no dilatation			
MOX Content (wgt.%)	HZP k_{eff}	HFP k_{eff}	$\Delta\rho/\Delta T$ (pcm/K)	Relative error	HZP k_{eff}	HFP k_{eff}	$\Delta\rho/\Delta T$ (pcm/K)	Relative error
1.0	1.07474	1.06403	-3.12	4.9%	1.08535	1.07497	-2.97	-0.3%
2.0	1.16395	1.15121	-3.17	4.3%	1.17496	1.16267	-3.00	-1.2%
4.0	1.23221	1.21820	-3.11	3.9%	1.24289	1.22936	-2.95	-1.5%
6.0	1.26934	1.25506	-2.99	3.5%	1.27949	1.26567	-2.84	-1.4%